NJC

PAPER

Cite this: *New J. Chem.*, 2018, 42, 6794

Ru(II)–thyminate complexes: new metallodrug candidates against tumor cells†

Rodrigo S. Correa,*[ab] Vitória Freire,[a] Marília I. F. Barbosa,[c] Daniel P. Bezerra,[d] Larissa M. Bomfim,[d] Diogo R. M. Moreira,[d] Milena B. P. Soares,[de] Javier Ellena[f] and Alzir A. Batista*[a]

Received 10th November 2017,
Accepted 24th March 2018

DOI: 10.1039/c7nj04368f

rsc.li/njc

Herein, we used thymine (HThy) as a ligand to form two new ruthenium(II) complexes with formula $[Ru(PPh_3)_2(Thy)(bipy)]PF_6$ (**1**) and $[Ru(Thy)(bipy)(dppb)]PF_6$ (**2**). The complexes were characterized by spectroscopic, spectrometric and X-ray crystallography analyses. Complexes **1** and **2** can interact with ctDNA presenting binding constants, K_b, of 0.4 and 1.2 × 10^3 M^{-1}, respectively. Their cytotoxic activities towards tumor cell lines (B16-F10, HepG2, K562 and HL-60) and non-tumor cells (PBMCs) were evaluated using the Alamar blue assay. Complex **1** exhibits high cytotoxicity against tumor cells, showing IC_{50} values of 0.01 and 1.81 μM against the HL-60 and HepG2 cell lines, respectively. Therefore, compound **1** can be considered as a promising antitumor metallodrug.

Introduction

Anticancer drug development based on transition metal complexes is an important line of investigation looking for new pharmaceuticals. Several classical anticancer metal-based drugs contain non-bioactive ligands, *i.e.* cisplatin, while non-classical antitumor metal complexes are composed of ligands endowed with pharmacological activity, such as natural compounds, DNA-binders, and enzyme-inhibitors.[1,2]

In recent years, transition metal complexes containing DNA nucleobase like compounds have been investigated as a strategy to understand how metals are able to interact with the DNA macromolecule.[3,4] Moreover, metal complexes containing a nucleobase can be used as a strategy for the rational design of bioactive molecules, acting as a Trojan horse for tumor cells, given that nucleobases are recognized by DNA polymerases and are used as DNA duplex building blocks.[5]

Accordingly, thymine (HThy) is an important biomolecule that consists of one of four nucleobase building blocks of DNA nucleic acids that is easily recognized by a biological system. Scheme 1 illustrates the molecular structure of HThy with atom numbering. The most stable form is the ketonic one, which can exist in equilibrium in the less stable enolic form.[6]

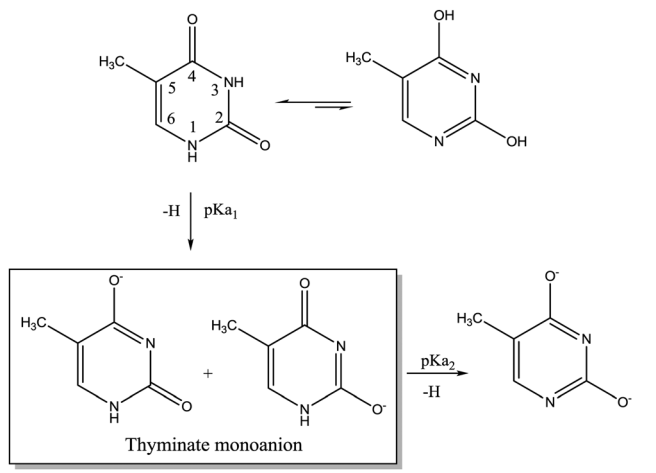

Scheme 1 Thymine structure, tautomeric equilibrium and anions (deprotonated from N3 and N1).

[a] *Departamento de Química, Universidade Federal de São Carlos – UFSCar, Rodovia Washington Luís KM 235, CP 676, 13561-901, São Carlos, SP, Brazil*
[b] *Departamento de Química, ICEB, Universidade Federal de Ouro Preto, CEP 35400-000, Ouro Preto, MG, Brazil. E-mail: rodricorrea@iceb.ufop.br; Tel: +55 3135591229*
[c] *Instituto de Química, Universidade Federal de Alfenas, CEP 37130-000, Alfenas, MG, Brazil*
[d] *Centro de Pesquisas Gonçalo Moniz, Fundação Oswaldo Cruz (CPqGM-FIOCRUZ-BA), Salvador, Bahia-BA, Brazil*
[e] *Centro de Biotecnologia e Terapia Celular, Hospital São Rafael, Salvador, Bahia-BA, Brazil*
[f] *Departamento de Física e Informática, Instituto de Física de São Carlos, Universidade de São Paulo, CP 369, 13560-970, São Carlos, SP, Brazil*

† Electronic supplementary information (ESI) available: PDF file of Table S1. Fig. S1 to S3 ($^{31}P\{^1H\}$, $^{13}C\{^1H\}$ and ^1H NMR spectra of complex **1**), S4 (infrared spectrum of complex 1), and S5 (electrochemical experiment for complex **1**). Fig. S6 to S8 ($^{31}P\{^1H\}$, $^{13}C\{^1H\}$ and ^1H NMR spectra of complex **2**), S9 (infrared spectrum of complex **2**), S10 (electrochemical experiment for complex **2**), S11 and S12 (fluorescence emission spectra of the BSA and HSA of **1** and **2**), and S13 (viscosity of ctDNA $(\eta/\eta_o)^{1/3}$ in the presence of complexes **1** and **2**). S14 (UV-Vis in DMSO/water of **1** and **2**). S15 and S16 ($^{31}P\{^1H\}$ of **1** and **2**) in DMSO/water. CCDC 1486728 and 1486729. For ESI and crystallographic data in CIF or other electronic format see DOI: 10.1039/c7nj04368f

The thymine molecule can be deprotonated, presenting monoanionic (Thy^-) and dianionic (Thy^{2-}) species. When the N3 atom is deprotonated, there are two possibilities to form monoanionic species,[6] as observed in Scheme 1. One presents the negative charge located on the C4–O^- and the other one is located on the C2–O^- group. Therefore, due to this structural versatility (Scheme 1), this molecule has many possibilities to react with metal ions in different modes, as can be observed for cytosine, another pyrimidine nucleobase.[7]

In coordination chemistry, thyminate(1−) can act as a versatile ligand in metal complexes, presenting different coordination modes and composition. Several compounds present thyminate coordinated by the N-heterocyclic N1 atom as monodentate, forming mononuclear complexes with Pt, Cu, Rh, W and Ir.[8] Even though less frequent the monodentate coordination mode involving the N3 atom can be found in complexes of Ag, Cu and Zn metal ions.[9] Dianionic thyminate(2−) occurs as a bridging ligand to give polynuclear complexes with Pt(II) and Rh(III) ions, in which N1, N3 and O2 atoms are involved in the coordination. The coordination of monocharged thyminate as bidentate is uncommon. This behaviour occurs frequently in metal complexes containing 1-methylthyminate derivatives, for example Pd(II)-based complexes with 1-methylthyminate-chelated form a strained Pd–N–C–O four membered ring.[10] Coordination compounds presenting a 2 : 1 : 1 ratio of metal/adenine/thymine, in which the metals are Mn(II), Co(II), Ni(II), Cu(II), Zn(II) and Cd(II), suggest that thymine coordinates the metal center as monodentate only through the O2 atom.[11]

In the literature, there are no ruthenium complexes with a thyminate ligand, motivating us to explore the behavior of this ligand with ruthenium. Recently, our research group has become interested in the chemical and biological behavior of ruthenium complexes with different phosphine and diimine ligands, as well as pharmaceutically active ligands such as natural products and drugs, as a strategy to design Ru(II)-based complexes endowed with antitumor, anti-parasitic, anti-tubercular and anti-xanthine oxidase activities.[12–16] Therefore, as part of our ongoing effort to design new anticancer compounds, in this paper, for the first time we used the DNA-building block, thyminate(1−), as a ligand for the ruthenium(II)/phosphine/diimine complex class. Furthermore, their biological properties were also evaluated.

Materials and methods

Materials, measurements and methods

All manipulations were performed under argon. The $RuCl_3{\cdot}3H_2O$, triphenylphosphine (PPh_3), 1,4-bis(diphenylphosphino)butane (dppb), 2,2′-bipyridine (bipy) and thymine (HThy) from Sigma-Aldrich were used as received. The *cis*-[$RuCl_2$(bipy)(PPh_3)$_2$] and *cis*-[$RuCl_2$(bipy)(dppb)] complexes were prepared according to the published procedure.[17,18]

The microanalyses were performed with an EA 1108 CHNS microanalyser (Fisons Instruments). The IR spectra were recorded on an FT-IR Bomem-Michelson 102 spectrometer in the range of 4000–250 cm^{-1} using CsI pellets. Conductivity data (presented as μS cm^{-1}) were obtained in CH_2Cl_2 using a Micronal model B-330 connected to Pt with constant cells equal to 0.089 cm^{-1}; measurements were made at room temperature using 1 mM solutions of the complexes. ^1H and ^{13}C NMR spectra were recorded on a Bruker DRX 400 MHz, internally referenced to TMS (tetramethylsilane), chemical shift (δ), multiplicity (*m*), spin–spin coupling constant (*J*), and integral (*I*). Acetone-d_6 was used as a solvent. The $^{31}P\{^1H\}$ chemical shifts are reported in relation to H_3PO_4 (85% v/v). The UV-Visible (UV-Vis) spectra of the complexes in CH_2Cl_2 were recorded on a Hewlett Packard diode array–8452A. Cyclic voltammetry experiments were carried out at 295 K, in CH_2Cl_2, containing 0.10 M Bu_4NClO_4 (tetrabutylammonium perchlorate, TBAP) (Fluka Purum), with a BAS-100B/W Bioanalytical Systems Inc electrochemical analyser. The working and auxiliary electrodes were stationary Pt foils; a Luggin capillary probe was used and the reference electrode was Ag/AgCl. Under these conditions, the ferrocene (Fc) is oxidized at 0.43 V (Fc^+/Fc).

Synthesis

To obtain complex **1**, the thymine nucleobase (23 mg; 0.18 mmol) was dissolved in a Schlenk flask with 50 mL of a mixture dichloromethane/methanol (1 : 1 v/v) containing triethylamine (10 μL) and KPF_6 (0.12 mmol; 15.0 mg). Next, 100 mg (0.12 mmol) of the precursor [$RuCl_2(PPh_3)_2$(bipy)] was added. The solution was kept under reflux, and an inert atmosphere, and was stirred for 48 h. The final solution was concentrated to *ca.* 2 mL, and 10 mL of water was added to precipitate an orange powder. The solids were filtered off, washed with warm water and diethyl ether separately, and dried under vacuum. Complex **2** was obtained from the same experimental procedure.

[Ru(PPh_3)$_2$(Thy)(bipy)]PF_6 (1)

Yield: 98 mg (80%). Anal. calc. for [$RuC_{51}H_{47}N_4O_4P_3F_6$]: exp. (calc.) C, 56.38 (56.20); H, 4.14 (4.53); N, 5.18 (5.14) %. Molar conductance (μS cm^{-1}, CH_2Cl_2) 40.1. IR (cm^{-1}): 3080, 3059, 2926, 2856, 1660, 1605, 1566, 1520, 1483, 1466, 1435, 1421, 1383, 1336, 1310, 1283, 1161, 1095, 1072, 1028, 999, 972, 902, 843, 742, 739, 698, 651, 530, 557, 517, 509, 493, 434, 417. $^{31}P\{^1H\}$ NMR (162 MHz, $CDCl_3$, 298 K): δ (ppm) 36.45 (s). ^1H NMR (400 MHz, acetone-d_6, 298 K): δ (ppm) 10.53 (1H, N–H of thy); 9.36–6.65 (30H atoms of PPh_3, 6H aromatic of bipy and 1H of thy); 1.24 (3H, methyl of thy). ^{13}C NMR (100 MHz, acetone-d_6, 298 K): δ (ppm) 181.15 (C2═O2); 159–104 (C-PPh_3; C-bipy, C-thy); 104.1 (C5 of thy); 10.09 (C_{methyl} of thy). UV-Vis (CH_2Cl_2, 4×10^{-4} M): λ/nm (ε/M^{-1} cm^{-1}) 296 (5590), 340 (1597), 440 (1081).

[Ru(Thy)(bipy)(dppb)]PF_6 (2)

Yield: 85 mg (70%). Anal. calc. For [$RuC_{44}H_{45}N_4O_3P_3F_6$]: exp. (calc.) C, 53.86 (53.50); H, 4.87 (4.80); N, 5.60 (5.67) %. Molar conductance (μS cm^{-1}, CH_2Cl_2) 51.7. IR (cm^{-1}): 3169, 3078, 3063, 2962, 2922, 2797, 1658, 1645, 1605, 1524, 1498, 1481, 1435, 1421, 1383, 1342, 1304, 1188, 1094, 1030, 999, 841, 761, 744, 696, 611, 557, 520, 492, 459, 420. $^{31}P\{^1H\}$ NMR (162 MHz, $CDCl_3$, 298 K): δ (ppm) 48.66 and 44.14 (d) [$^2J_{p-p}$ = 32.42 Hz]. ^1H NMR (400 MHz, acetone-d_6, 298 K): δ (ppm) 9.26 (1H, N–H of

thy); 8.58–6.05 (24H atoms of dppb, 6H aromatic of bipy and 1H of thy); 3.17–1.62 (8H-$_{CH_2}$ of dppb); 0.87 (3H, methyl of thy). ^{13}C NMR (100 MHz, acetone-d$_6$, 298 K): δ (ppm) 183.73 (C4═O4); 161–123 (C-PPh$_3$; C-bipy, C-thy); 105.9 (C5 of thy); 10.10 (C–$_{methyl}$ of thy). UV-Vis (CH_2Cl_2, 10^{-5} M): λ/nm (ε/M^{-1} cm^{-1}) 282 (7500), 420 (1311).

X-ray structure determination

Orange single-crystals of complexes **1** and **2** were grown by evaporating a methanol/water (10 : 1 v/v) solution. Room temperature (298 K) X-ray diffraction experiments were carried out on an Enraf–Nonius Kappa-CCD diffractometer with graphite monochromated MoKα radiation (λ = 0.71073 Å). The cell refinements were performed using the software Collect[19] and Scalepack,[20] and final cell parameters were obtained on all reflections. Data reduction was carried out using the software Denzo-SMN and Scalepack.[20] The structures were solved by the direct method using SHELXS-97[21] and refined using the software SHELXL-97.[21] The Gaussian method was used for the absorption corrections.[22] Tables and structure representations were generated by WinGX[23] and MERCURY,[24] respectively. The main crystal data collections and structure refinement parameters for **1** and **2** are summarized in Table 1. Non-hydrogen atoms of the complexes were unambiguously located, and a full-matrix, least-squares refinement of these atoms with anisotropic thermal parameters was carried out.

In all ligands of complexes **1** and **2**, the aromatic C–H hydrogen atoms were positioned stereochemically and were refined with fixed individual displacement parameters [U_{iso}(H) = 1.2U_{eq}(Csp^2)] using a riding model with aromatic C–H bond lengths fixed at 0.93 Å. Methylene groups of dppb of complex **2** were also set as isotropic with a thermal parameter 20% greater than the equivalent isotropic displacement parameter of the atom to which each one was bonded, and the C–H bond lengths were fixed at 0.97 Å. H atoms bound to the C61 methyl group were located from an electron-density difference analysis and refined as riding on their parent atoms, with U_{iso}(H) values of 1.5 U_{eq}(C) for methyl H atoms.

DNA titration and viscosity experiments

DNA/complex interactions were evaluated by UV-Vis spectroscopic titration. A solution of calf thymus DNA (ctDNA), from Sigma-Aldrich, was prepared in a Tris–HCl buffer (5 mM Tris–HCl, pH 7.4). The concentration of this standard ctDNA solution was measured from its absorption intensity at 260 nm, using the molar absorption coefficient value of 6600 M^{-1} cm^{-1}. We found that the ctDNA solution is protein-free, given that the ratio of UV absorbance at 260 and 280 nm is about 1.8 : 1. The solution of ruthenium complexes used in the experiments was prepared in a Tris–HCl buffer containing 5% DMSO. It is worth mentioning that the structure of complex 1 changes after its incubation in a DMSO/water medium, such as observed in the ultraviolet-visible and ^{31}P{^{1}H} NMR spectra (see the ESI†). The observed change can be attributed to exchange of the PPh$_3$ ligand by DMSO or water molecules, since the signal of free PPh$_3$ is observed in the ^{31}P{^{1}H} NMR spectrum, at around −6 ppm.

In the titration experiments, different concentrations of the ctDNA were used while the ruthenium complex was at 20 μM. A sample correction was made for the absorbance of ctDNA and the spectra were recorded. The intrinsic equilibrium binding constant (K_b) of the complexes to ctDNA was obtained by monitoring changes in the absorption intensity with an increasing

Table 1 Crystal data and structure refinement parameters obtained for complexes **1** and **2**

	1	**2**
Empirical formula	$RuC_{51}H_{43}N_4O_2P_3F_6$	$RuC_{43}H_{48}N_4O_4P_2$
Formula weight	1051.87	843.83
Crystal system	Triclinic	Monoclinic
Space group	$P\bar{1}$	$P2_1/n$
Unit cell dimensions		
a (Å)	13.107(1)	18.3197(7)
b (Å)	13.733(1)	12.5109(7)
c (Å)	14.608(1)	19.7938(16)
α (°)	81.323(3)	90
β (°)	70.114(4)	116.165(3)
γ (°)	75.816(3)	90
Volume (Å^3)	2390.7(3)	4071.8(4)
Z	2	4
Density calculated (Mg m^{-3})	1.461	1.406
μ (mm^{-1})	0.497	0.513
F(000)	1072	1784
Crystal size (mm^3)	0.13 × 0.30 × 0.35	0.10 × 0.14 × 0.30
θ range (°)	2.92 to 26.37°	2.96 to 26.38°
Index ranges	$-16 \le h \le 16$; $-17 \le k \le 16$; $-18 \le l \le 18$	$-22 \le h \le 22$; $-15 \le k \le 15$; $-24 \le l \le 24$
Reflections collected	18 047	27 984
Independent reflections	9744 [R(int) = 0.0234]	8240 [R(int) = 0.0650]
Completeness to θ (%)	99.5	98.7
Data/restraints/parameters	9744/197/638	8240/153/494
Goodness-of-fit on F^2	1.027	1.056
Final R indices [$I > 2$sigma(I)]	R_1 = 0.0489, wR_2 = 0.1351	R_1 = 0.0590, wR_2 = 0.1410
R indices (all data)	R_1 = 0.0591, wR_2 = 0.1432	R_1 = 0.0890, wR_2 = 0.1555
$\Delta\rho_{max}$; $\Delta\rho_{min}$ (e Å^{-3})	1.087 and −0.837	0.581 and −0.622

concentration of ctDNA, and was analysed by regression analysis. Viscometric titrations of 1 and 2 were performed using an Ostwald viscometer at a constant temperature (310 K). For comparison, ctDNA was also incubated with thiazole orange (TO), an effective intercalator. The concentration of ctDNA was 1.2×10^{-3} μM, and the flow times were measured with an automated timer. Each sample was measured 5 times and an average flow time was calculated. Data were presented as $(\eta/\eta_0)^{1/3}$ *versus* [complex]/[ctDNA], where η is the viscosity of ctDNA in the presence of the complex and η_0 is that of ctDNA alone. Relative viscosity for ctDNA in either the presence or absence of the complex was calculated from the relation: $\eta = (t - t_0)/(t_0)$, where t is the observed flow time of the ctDNA containing solution and t_0 is the flow time of the buffer alone.

Cytotoxicity assay

Cytotoxicity was evaluated against tumor cells lines B16-F10 (mouse melanoma), HepG2 (human hepatocellular carcinoma), K562 (human chronic myelocytic leukemia) and HL-60 (human promyelocytic leukemia). All cell lines were donated by the A. C. Camargo Hospital, São Paulo, SP, Brazil. The cells were maintained in Roswell Park Memorial Institute-1640 (RPMI-1640, Gibco-BRL) medium, supplemented with 10% fetal bovine serum (Cultilab), 2 mM L-glutamine (Vetec Química Fina) and 50 μg mL^{-1} gentamycin (Novafarma). Adherent cells were harvested *via* treatment with a 0.25% trypsin EDTA solution (Gibco-BRL). All cell lines were cultured in cell culture flasks at 310 K in 5% CO_2 and sub-cultured every 3–4 days to maintain exponential growth. All experiments were conducted with cells in the exponential growth phase. All cell lines were tested for mycoplasma using the Lookout® Mycoplasma qPCR detection kit (Sigma-Aldrich), and all cells were shown to be free from contamination.

The compounds were also tested against a non-tumor cell, human lymphoblast cells. Heparinized blood (from healthy 20–35 year old non-smoker donors who had not taken any drugs at least 15 days prior to sampling) was collected and peripheral blood mononuclear cells (PBMCs) were isolated by a standard protocol using a Ficoll density gradient in a GE Ficoll-Paque Plus. The PBMCs were washed and resuspended at a concentration of 0.3×10^6 cells per mL in an RPMI 1640 medium supplemented with 20% fetal bovine serum, 2 mM glutamine, 50 μg mL^{-1} gentamycin at 310 K with 5% CO_2. In addition, concanavalin A (ConA; Sigma Chemical Co) was used as a mitogen to trigger cell division in T-lymphocytes. ConA (10 μg mL^{-1}) was added at the beginning of the culture and, after 24 h, the cells were treated with the test drugs. The Research Ethics Committee of the Fundação Oswaldo Cruz (Salvador, Bahia, Brazil) approved the experimental protocol (#031019/2013). All participants signed their written informed consent to participate in the study. For all experiments, cell viability was performed by the Trypan blue exclusion assay. Over 90% of the cells were viable at the beginning of the culture.

Cell viability was quantified by the Alamar blue assay.[25] For all experiments, cells were seeded in 96-well plates (0.7×10^5 cells per mL for adherent cells or 0.3×10^6 cells per mL for suspended cells in 100 μL of medium). After 24 h, the compounds (0.04–25 μg mL^{-1}) dissolved in dimethyl sulfoxide (DMSO, Sigma Chemical Co), were added to each well and incubated for 72 h. Doxorubicin (purity ≥ 95.0%, doxorubicin hydrochloride, Laboratory IMA S.A.I.C) and oxaliplatin (purity 100%, Sigma-Aldrich) were used as the positive control (0.04–5 μg mL^{-1}). The negative control received the vehicle used for diluting the tested compounds (0.5% DMSO). Four (for cell lines) or 24 (for PBMC) hours before the end of the incubation, 20 μL of the stock solution (0.312 mg mL^{-1}) of Alamar blue (resazurin, Sigma-Aldrich Co) was added to each well. The absorbance was measured using a SpectraMax 190 multiplate reader and the drug effect was quantified as the percentage of control absorbance at 570 nm and 600 nm. Data were presented as half maximal inhibitory concentration (IC_{50}) values ±S.E.M. obtained by nonlinear regression from three independent experiments performed in duplicate. All analyses were carried out using the GRAPHPAD software (Intuitive Software for Science).

Results and discussion

Synthesis

Reactions of *cis*-$[RuCl_2(PPh_3)_2(bipy)]$ and *cis*-$[RuCl_2(bipy)(dppb)]$ with thymine lead to new complexes $[Ru(PPh_3)_2(Thy)(bipy)]PF_6$ (**1**) and $[Ru(Thy)(bipy)(dppb)]PF_6$ (**2**). The synthetic step used in this work provided good yield with satisfactory elemental analysis data (see Experimental section). The molar conductance measurements for the compounds are consistent with 1 : 1 type compounds,[26] suggesting that after the exchange of two chlorine ligands, the Thy^- ligand is coordinated to the Ru(II) metal as monoanionic.

Crystal structure and molecular assembly of complexes 1 and 2

The X-ray crystallographic studies confirm the presence of one molecule of thymine coordinated, as a bidentate ligand, in each compound. Furthermore, complex **1** presents one 2,2′-bipyridine and two triphenylphosphine ligands, while complex **2** presents one bisphosphinic ligand instead of two PPh_3. As seen in Fig. 1, the proposed formulae for **1** and **2** were confirmed. It should be emphasized that this report represents the first report of structure determination by X-ray crystallography of thymine/ruthenium complexes.

Both structures form a slightly distorted octahedral geometry, highlighted by the bond angles around the metal centers (Table 2). In the two complex structures, the N2–Ru–N4 and N3–Ru–O1 bond angles are far from the expected value of 90° due to the tension of the five- and four-membered chelate rings of the bipy and thymine ligands, respectively. In complex **1**, the P–Ru–N and P1–Ru–P2 (PPh_3 ligands adopting a *trans* configuration) bond angles are close to 90° and 180°, respectively (see Table 2). Furthermore, it is observed that the $Ru–N_{bipy}$ and Ru–P bond lengths are in agreement with the values presented in complexes obtained from the literature, mainly those ones from the same Ru(II) precursors.[9,11,13,27]

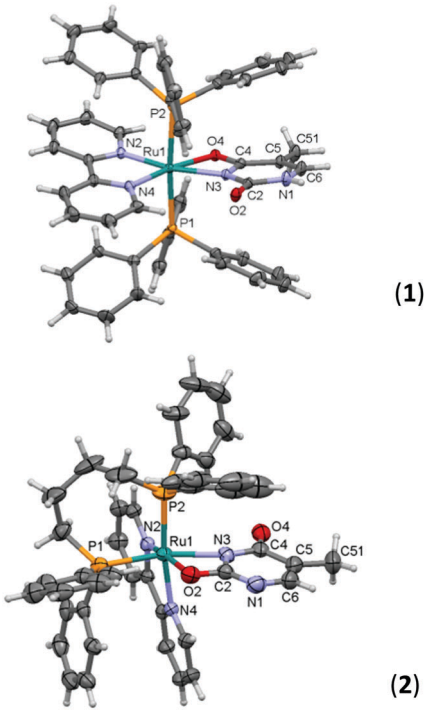

Fig. 1 Molecular geometries for complexes **1** and **2**, presenting the selected atoms labeled and ellipsoids at 30% probability. For the sake of clarity, the PF_6^- counterion was omitted.

Table 2 Selected bond lengths and angles (Å, °) for **1** and **2** and compared with free thymine

Fragment	1	2	Free thymine[23]
Thymine moiety			
*d*C2–O2	1.245(3)	1.292(5)	1.244(4)
*d*C4–O4	1.279(3)	1.253(6)	1.225(4)
*d*C2–N3	1.351(3)	1.345(6)	1.361(4)
*d*C4–N3	1.359(3)	1.341(6)	1.401(5)
*d*C2–N1	1.376(3)	1.343(6)	1.358(4)
*d*C4–C5	1.422(4)	1.444(7)	1.453(4)
*d*C5–C6	1.346(4)	1.334(8)	1.343(4)
*d*C6–N1	1.353(4)	1.353(8)	1.384(5)
Metal center			
*d*Ru1–O2	—	2.120(3)	
*d*Ru1–O4	2.156(2)	—	
*d*Ru1–N2	2.038(2)	2.074(3)	
*d*Ru1–N3	2.130(2)	2.153(3)	
*d*Ru1–N4	2.045(3)	2.104(3)	
*d*Ru1–P1	2.3885(7)	2.309(1)	
*d*Ru1–P2	2.4128(7)	2.299(1)	
≤O2–Ru1–N2	—	165.12(12)	
≤O2–Ru1–N3	—	61.77(14)	
≤O4–Ru1–N2	107.25(8)	—	
≤O4–Ru1–N3	61.58(7)	—	
≤N2–Ru1–N3	167.46(9)	108.78(13)	
≤P1–Ru1–P2	175.04(2)	95.08(5)	
≤N3–Ru1–P1	90.20(7)	162.77(11)	
≤P2–Ru1–N4	94.49(7)	172.83(9)	

The crystal structure of free thymine was previously published,[23,24] and the main bond values are also represented in Table 2, in which the C2═O2 (1.244 Å) and C4═O4 (1.225 Å) bond lengths indicate a double-bond character, whereas the C2–N1, C2–N3 and C4–N3 bonds are single bonds (1.358–1.401 Å). Comparing these values with the crystal structure of complex **1**, in which the thymine ligand is coordinated by the N3 and O4 atoms, the bond lengths C4–O4 present significant lengthening and C4–N3 shortening (see Table 2). On the other hand, complex **2** which presents different coordination modes, with thymine coordination through N3 and O2 atoms, the bond length C2–O2 presents significant lengthening and C2–N3 shortening. In both cases, the presence of monoanionic charge on the ligand can be observed, which can be delocalized over the fragment $[O–Ru–N–C]^-$. Moreover, we attribute that the different stereochemistry around the metal in each precursor contributes to driving forces to stabilize thymine coordination in different modes, as observed in **1** and **2**.

The crystal structure of free thymine exhibits patterns with bifurcated N–H···O hydrogen bonding and C–H···O interactions forming infinite chains.[28] However, only the crystal structure of complex **1** is maintained by bifurcated N–H···O hydrogen bonding (see Fig. 2). To stabilize the crystal structure of complex **2**, weak π···π contacts, as well as hydrogen bonds with water molecules are present (Fig. 3).

Infrared and ultraviolet-visible spectroscopy

In the IR spectrum of the Thy ligand, two bands are observed related to N3–H and N1–H, however in the IR spectra of complexes **1** and **2** (see the ESI†), only one *ν*N–H stretching band is observed at around 3200 cm^{-1}, suggesting that one of the nitrogen atoms is coordinated after it is deprotonated.

In addition, the free thymine presents two intense bands in the region between 1800 and 1610 cm^{-1}, which are assigned to *ν*C═O stretching vibrations.[29] One band occurs at 1743 cm^{-1} and another at around 1680 cm^{-1}. In complexes **1** and **2**, only one band related to *ν*C═O stretching vibrations occurs at around 1658 and 1660 cm^{-1}, respectively. The absence of the *ν*C═O band in the spectra of the complexes is evidence of ligand coordination; however, this information does not contribute to confirming which C═O group is coordinated to ruthenium in each complex. Strong bands in the region of 1550–1300 cm^{-1} are characteristic of *ν*C═N and *ν*C═C stretching vibrations and are present in the spectra of the ligand and complexes. The presence of the phosphine ligand is confirmed by the *ν*P–C at about 1090 cm^{-1}.

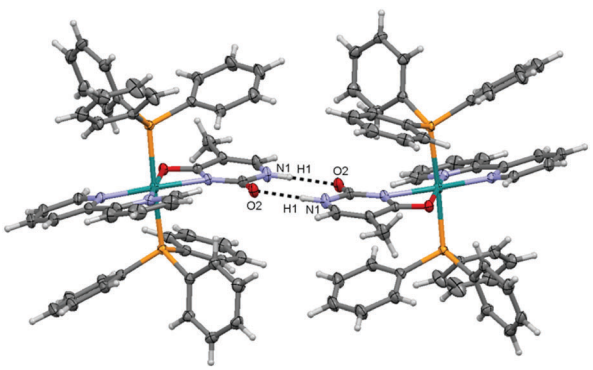

Fig. 2 N–H···O hydrogen bonding stabilizing the structure of complex **1**.

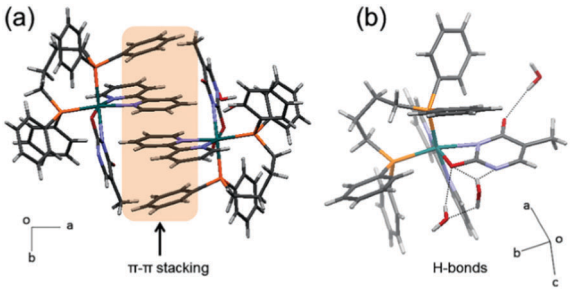

Fig. 3 Intermolecular interactions stabilizing the structure of complex **2**: (a) π–π stacking interaction and (b) hydrogen bonds between the complex and water molecules.

The complexes exhibit νRu–P stretching in the range of 521–511 cm^{-1}. Moreover, νRu–N and νRu–O stretching vibrations occur as very weak bands in a region of low intensity at about 500–350 cm^{-1}.

Electronic spectra of the two complexes were obtained in dichloromethane solutions. The transitions found in the range of 282–296 nm ($\varepsilon \sim 6000$ mol^{-1} L cm^{-1}) correspond to intraligand (IL) transitions; meanwhile transitions at around 430 nm, in both complexes, and at 340 in complex **1** (with $\varepsilon \sim 1000$ mol^{-1} L cm^{-1}), are assigned to metal–ligand charge transfer (MLCT) transition.

Multinuclear $^{31}P\{^1H\}$, ^1H and ^{13}C NMR experiments

In the ^1H NMR spectrum of the free thymine, two shoulder bands corresponding to a singlet of the N–H group proton are observed in the region of 11.0–10.60 ppm. Only one signal is present in the spectra of the complexes (10.25–9.35 ppm) (see the ESI†), indicating the deprotonation of one nitrogen atom of thymine after its coordination with the metal. Additionally, the ^1H NMR spectra of complexes **1** and **2** showed the characteristic deshielded signal at 9–8 ppm, corresponding to the *ortho* hydrogen atoms of the bipy ligand. Other aromatic hydrogen atoms of phosphine and bipy ligands present signals in the range of 6.28–7.94 ppm, including the singlet of the H-atom bonded to the C6 atom of the Thy ligand. All complex spectra exhibit a singlet at 1.27–0.85 ppm assigned to the methyl group of thymine.

The ^{13}C NMR spectrum of complex **1** shows a signal at 181.1 ppm assigned to the carbon atom of the non-coordinated C2═O2 group, meanwhile in complex **2**, the carbon atom of the non-coordinated C4═O4 group occurs at 183.7 ppm. For the free ligand, these signals of C2═O2 and C4═O4 groups occur at about 183 and 170 ppm, respectively.

Aromatic carbon atoms of the bipy, phosphine and thymine ligands were also identified in the range of 161–123 ppm. In the spectra of the complexes, the signals in the range of 104–105 ppm belong to the C5 carbon atom of the thymine. Complex **2** presents signals at around 23–28 ppm assigned to carbon atoms of the CH_2 groups of the dppb ligand. Both complexes exhibit a characteristic signal of the methyl group of thymine at around 10.1 ppm.

Finally, the $^{31}P\{^1H\}$ experiment for complex **1** shows the presence of one singlet signal for coordinated phosphorus of each complex around 36 ppm due to the equivalence of the two phosphorus atoms in the *trans* configuration.[9,11,23,30] On the other hand, the $^{31}P\{^1H\}$ spectrum of complex **2** presents two doublet signals, indicating the presence of two non-equivalent phosphorus atoms. These signals, in the region of 48.66 and 44.14 ppm ($^2J_{p-p}$ = 32.42 Hz) are consistent with one phosphorus atom of dppb *trans* to the nitrogen atom of bipy and another phosphorus of dppb *trans* to one N-atom of thymine.[10,14] In the $^{31}P\{^1H\}$ spectra of complexes **1** and **2**, heptet signals of the PF_6^- anion around −144 ppm were observed.

Electrochemical studies

The electrochemical behavior of the complexes containing the thymine ligand in cyclic voltammetry experiments were similar to those found for other Ru(II) complexes that present monophosphine as ligands in a *trans* configuration[9,11,23] and others containing {Ru-dppb} reported elsewhere.[10] These experiments were performed under the same conditions and it was observed that complexes **1** and **2** exhibit a quasi-reversible redox process assigned to one-electron Ru(II)/Ru(III), with E_{pa} of 1125 and 1260 mV, respectively. The difference observed between the complexes may be due to the different stereochemistry found for them. The $E_{1/2}$ values found for the complexes were considerably more anodic than those observed for both precursors $[RuCl_2(PPh_3)_2(bipy)]$[13] and $[RuCl_2(bipy)(dppb)]$,[14] indicating that the ruthenium center is more stable after coordination of thymine compared with the precursor. The metal center stabilization occurs due to the exchange of two chlorides by a negatively charged Thy chelating ligand.

DNA-binding: UV-Vis spectrophotometric titration and viscosity studies

Binding studies between DNA and ruthenium complexes with antitumor activity have been extensively performed to better understand the mechanism of action.[31] The two complexes exhibit the same behavior when ctDNA is added (Fig. 4), in which absorption spectra decrease at the rate of about 45 and 15%, respectively, suggesting that interactions occur between the complexes and DNA. The magnitude of this interaction was analysed by DNA binding constants, K_b, which were calculated according to eqn (1):

$$[ctDNA]/(\varepsilon_a - \varepsilon_f) = [ctDNA]/(\varepsilon_b - \varepsilon_f) + 1/K_b(\varepsilon_b - \varepsilon_f) \quad (1)$$

in which [ctDNA] is the concentration of ctDNA in base pairs, ε_a is the ratio of the absorbance/[Ru], ε_f is the extinction coefficient of the free Ru(II) complex, and ε_b is the extinction coefficient of the complex in the fully bound form. The ratio of the slope to the intercept in the plot of $[DNA]/(\varepsilon_a - \varepsilon_f)$ *vs.* [DNA] gives the value of K_b, which was calculated from the metal to ligand charge transfer (MLCT) absorption band (λ_{max}) at around 420 nm.

The compounds $[Ru(PPh_3)_2(Thy)(bipy)]PF_6$ (**1**) and [Ru(Thy)-(bipy)(dppb)]PF_6 (**2**) interact with DNA presenting binding constants, K_b, of 4.0×10^3 and 1.2×10^3 M^{-1}, respectively. These K_b values are very close between them, and complex **1** presents a K_b slightly higher than that of complex **2**. The similar magnitude of K_b found here, is comparable with those for metal

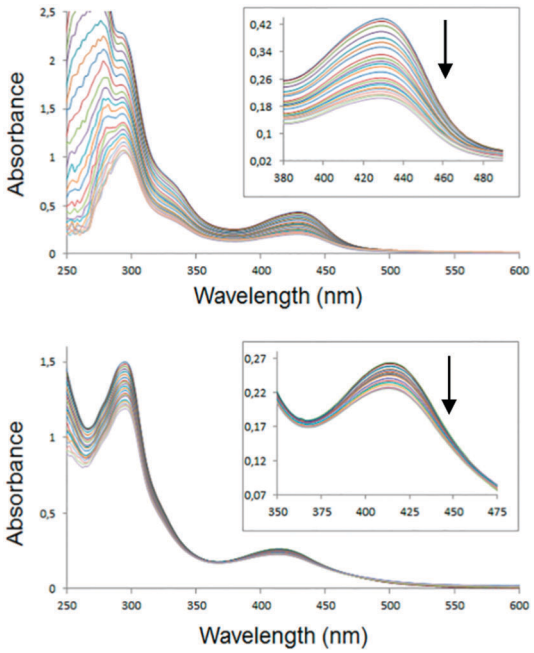

Fig. 4 Changes in the electronic absorption spectra of complexes **1** (top) and **2** (bottom) with an increasing concentration of ctDNA.

complexes with non-covalent (electrostatic or hydrogen bonding) interactions with ctDNA reported in the literature (K_b ranging from 10^{-3} to 10^{-4} M^{-1}).[30–33] Therefore, complexes **1** and **2** can interact with DNA by non-covalent modes, such as what occurs with other Ru(II)/phosphinic/diiminic complexes reported elsewhere.[8,11] In solution, DNA-complex affinity can be kept by electrostatic interaction and/or N–H···O hydrogen bonds that are observed in the solid state forms for the complex molecules (see Fig. 2).

Furthermore, the viscosity of ctDNA was followed by increasing the concentration of Ru(II) complexes **1** and **2**, in which small changes can be observed when compared to changes caused by the intercalation agent thiazole orange (see the ESI,† Fig. S13). Complex **1** increased the ctDNA viscosity slightly compared to complex **2**, supporting the slightly higher K_b value of **1** than **2**. In both cases, the ruthenium complexes present just a weak interaction, possible either by an electrostatic mode or hydrogen bonding.[31–33]

HSA and BSA binding studies of complexes 1 and 2

In this paper, the interactions of complexes **1** and **2** with both human serum albumin (HSA) and bovine serum albumin (BSA) were evaluated by fluorescence quenching. It is worth mentioning that BSA and HSA, which are transport proteins, have very similar chemical structures. Therefore, the ability of compounds to bind BSA and HSA has been widely studied in order to better understand if the active molecules can be transported by this type of protein to the biological target.[33]

The experiments were carried out by adding the ruthenium(II) complexes **1** or **2** to the HSA or BSA solution at two different temperatures: 295 and 310 K, following the fluorescence intensity suppression. Table 3 shows the constant values obtained for both complexes **1** and **2**. The magnitude of the HSA and BSA-binding constants of both compounds compared with other Ru(II) compounds reported recently suggests a moderate interaction with both molecules.[8,11]

The thermodynamic parameters (ΔH°, ΔS° and ΔG°) were analyzed to evaluate the intermolecular forces involving the molecules of the complexes and the proteins. The negative values of ΔG° in all situations indicate a spontaneous interaction between them. In addition, as the complexes present regions to be hydrogen bonded (around thymine ligand) and also hydrophobic regions (around dppb and bipy ligands), these kinds of interactions can occur between the HSA/BSA and the complexes. As indicated by the sign and magnitude of the thermodynamic parameters, the $\Delta H^\circ < 0$ and $\Delta S^\circ < 0$ correspond to hydrogen bonding interactions, the values for $\Delta H^\circ > 0$ and $\Delta S^\circ > 0$ imply the involvement of hydrophobic forces in protein binding and $\Delta H^\circ < 0$ and $\Delta S^\circ > 0$ suggests the presence of electrostatic forces.[34] As observed in Table 3, when we analyze the interaction occurring in **1**-HSA and **2**-BSA, positive ΔS° and negative ΔH° values are found that indicate the presence of electrostatic forces in these cases.

On the other hand, different interactions were observed in the study involving the **2**-HSA and **1**-BSA, with positive ΔS° and ΔH° values, suggesting the presence of hydrophobic forces between the protein and the aliphatic regions of the complexes, probably around the diiminic and phosphinic ligands. This kind of interaction is possible when aromatic groups are present, as illustrated in Fig. 3a. The hydrophobic forces, which occurred in both **2**-HSA and **1**-BSA systems, are stronger than electrostatic interactions in **1**-HSA and **2**-BSA, as can be observed by the slightly higher K_b values found for **2**-HSA and **1**-BSA. As a result, complex **2** interacts more strongly with HSA than complex **1**, while complex **1** interacts more strongly with BSA than complex **2**. The magnitude of the K_b values of complexes **1** and **2**, compared with other Ru(II) complexes reported recently,[11] suggests a moderate interaction with serum

Table 3 The quenching constants (K_{SV}), (k_q), binding constants (K_b), number of binding sites (n) and the thermodynamic parameters obtained from complexes **1** and **2** with HSA and BSA at different temperatures (295 and 310 K)

Compound/albumin	T (K)	$K_{sv} \times 10^4$ (M^{-1})	$k_q \times 10^{12}$ (M^{-1} s^{-1})	$K_b \times 10^5$ (M^{-1})	N	ΔH° (kJ mol^{-1})	ΔS° (J mol^{-1} K^{-1})	ΔG° (kJ mol^{-1})
1/HSA	295	4.3 ± 0.2	6.93	0.8 ± 0.3	1.1	−4.24	79.43	−27.91
	310	4.5 ± 0.3	7.25	0.73 ± 0.3	1.1			−28.86
2/HSA	295	3.3 ± 0.2	5.32	3.7 ± 0.8	1.2	9.61	138.82	−31.76
	310	3.2 ± 0.02	5.16	4.3 ± 0.5	1.3			−33.43
1/BSA	295	5.2 ± 0.1	8.39	18.0 ± 0.1	1.3	3.43	131.96	−35.68
	310	4.9 ± 0.3	7.90	19.0 ± 0.1	1.3			−37.26
2/BSA	295	3.4 ± 0.2	5.48	1.7 ± 0.8	1.2	−8.01	73.25	−29.84
	310	3.5 ± 0.1	5.64	1.5 ± 0.5	1.2			−30.72

Table 4 *In vitro* cytotoxic activity of the ruthenium complexes **1** and **2**

	IC_{50}[a] (μM)				
Cell lines	**1**	**2**	Thymine	Doxorubicin[b]	Oxaliplatin[b]
Tumor cells[c]					
B16-F10	0.01 ± 0.02	9.87 ± 3.47	>100	0.04 ± 0.02	0.04 ± 0.02
HepG2	1.81 ± 0.49	>20	>100	0.08 ± 0.04	0.50 ± 0.13
HL-60	0.01 ± 0.01	9.98 ± 1.89	>100	0.03 ± 0.02	0.40 ± 0.23
K562	0.10 ± 0.30	2.87 ± 0.89	>100	0.10 ± 0.04	0.38 ± 0.11
Non-tumor cells[d]					
PBMC	1.19 ± 0.38	10.47 ± 3.78	>100	5.41 ± 1.37	42.40 ± 9.70

[a] Data are presented as IC_{50} values ± S.E.M., in μM, obtained by nonlinear regression from three independent experiments performed in duplicate, measured by Alamar blue assay after 72 h of incubation. [b] Doxorubicin and oxaliplatin were used as the positive control. [c] Tumor cells: B16-F10 (mouse melanoma), HepG2 (human hepatocellular carcinoma), HL-60 (human promyelocytic leukemia) and K562 (human chronic myelocytic leukemia). [d] Non-tumor cells: PBMCs (human peripheral blood mononuclear cells activated with concanavalin A – human lymphoblast).

albumin, which is desired. Thus, the molecules of complexes **1** and **2** can be stored in protein and released at targets.

In vitro cytotoxic activity of complexes 1 and 2

The *in vitro* cytotoxic effects of the ruthenium complexes **1** and **2** were assessed in tumor and non-tumor cells using the Alamar blue assay after 72 h of incubation (Table 4). Complex **1** exhibited potent cytotoxicity in relation to positive controls (doxorubicin and oxaliplatin), and its IC_{50} value is comparable to those obtained for ruthenium(II)-based 5-fluorouracil complex containing PPh_3, recently reported.[35]

The IC_{50} values for complex **1** ranged from 0.01 to 1.81 μM for the HL-60 and HepG2 tumor cell lines (Table 4). Doxorubicin and oxaliplatin showed IC_{50} values ranging from 0.03 to 0.10 μM for the HL-60 and K562 tumor cell lines and from 0.04 to 0.50 μM for the B16-F10 and HepG2 tumor cell lines, respectively. Importantly, free thymine was not cytotoxic in tumor cell lines, with IC_{50} values greater than 100 μM. Complex **1** was 119 fold more active against HL-60 cells than against peripheral blood mononuclear cells (PBMCs). Meanwhile, doxorubicin and oxaliplatin were 180 and 106 fold more potent, respectively, against HL-60, than the PBMC cell line.

Conclusions

This report presents the first examples of ruthenium(II) complexes with the thymine nucleobase: $[Ru(PPh_3)_2(Thy)(bipy)]PF_6$ (**1**) and $[Ru(Thy)(bipy)(dppb)]PF_6$ (**2**). Their synthesis, characterization, HSA/BSA/DNA-binding studies and cytotoxicity analysis were carried out. The crystal structures of the ruthenium(II)/thymine complexes were determined confirming that thymine can coordinate with Ru(II) in different modes. The studies on complex/DNA binding provide low DNA-binding constants with binding constants of around 10^3 M^{-1}. In addition, complex **1** exhibited potent cytotoxicity in relation to the positive controls, doxorubicin and oxaliplatin, indicating that this molecule is a promising metallodrug against tumor cells. The results suggest that the thymine Ru(II) complex interacts with DNA through weak interactions. Therefore, to determine the possible mechanisms of action, further experiments are ongoing in our laboratory.

Conflicts of interest

There are no conflicts to declare.

Acknowledgements

We would like to thank the Brazilian Research Council CNPq, FAPEMIG, FAPESB and FAPESP. R. S. Correa would like to thank CNPq for financial support (project 403588/2016-2 and 308370/2017-1).

References

1 J. Qin, R. Rajaratnam, L. Feng, J. Salami, J. S. Barber-Rotenberg, J. Domsic, P. Reyes-Uribe, H. Liu, W. Dang, S. L. Berger, J. Villanueva, E. Meggers and R. Marmorstein, *J. Med. Chem.*, 2015, **58**(1), 305.
2 P. Martins, M. Marques, L. Coito, A. J. Pombeiro, P. V. Baptista and A. R. Fernandes, *Anticancer Agents Med. Chem.*, 2014, **14**(9), 1199.
3 B. García, J. Garcia-Tojal, R. Ruiz, R. Gil-García, S. Ibeas, B. Donnadieu and J. M. Leal, *J. Inorg. Biochem.*, 2008, **102**, 1892.
4 M. Nath, H. Singh, G. Eng, X. Song and A. Kumar, *Inorg. Chem. Commun.*, 2009, **12**, 1049.
5 R. E. Johnson, S. Prakash and L. Prakash, *Science*, 1999, **283**, 5404.
6 S. Ganguli and K. K. Kundu, *Can. J. Chem.*, 1994, **72**, 1120.
7 W. Bruning, I. Ascaso, E. Freisinger, M. Sabat and B. Lippert, *Inorg. Chim. Acta*, 2002, **339**, 400.
8 (*a*) R. Faggiani, B. Lippert, C. J. L. Lock and R. Pfab, *Inorg. Chem.*, 1981, **20**, 2381; (*b*) T. J. Kistenmacher, T. Sorell and L. G. Marzilli, *Inorg. Chem.*, 1975, **14**, 2479; (*c*) M. Sakate, A. Kashima, H. Hosoda, Y. Sunatsuki, H. Ota, A. Fuyuhiro and T. Suzuki, *Inorg. Chim. Acta*, 2016, **452**, 205; (*d*) R. Kramer, K. Polborn and W. Beck, *J. Organomet. Chem.*, 1991, **410**, 111; (*e*) D. J. Darensbourg, B. J. Frost,

D. L. Larkins and J. H. Reibenspies, *Eur. J. Inorg. Chem.*, 2000, 2487.
9 (*a*) P.-S. Nong, Y.-F. Zhou, L.-H. Huang, J.-D. Lou, X.-H. Chen and X. L. Lu, *Synth. React. Inorg., Met.-Org., Nano-Met. Chem.*, 2012, **42**, 313; (*b*) M. Parvez and W. J. Birdsall, *Acta Crystallogr., Sect. C: Cryst. Struct. Commun.*, 1994, **50**, 540; (*c*) G. Gasser, M. J. Belousoff, A. M. Bond, Z. Kosowski and L. Spiccia, *Inorg. Chem.*, 2007, **46**, 1665.
10 J. Ruiz, M. D. Villa, V. Rodríguez, N. Cutillas, C. Vicente, G. Lopez and D. Bautista, *Inorg. Chem.*, 2007, **46**, 14.
11 R. Ghose, *Synth. React. Inorg. Met.-Org. Chem.*, 1992, **22**(4), 379–392.
12 (*a*) M. S. de Camargo, M. M. da Silva, R. S. Correa, S. D. Vieira, S. Castelli, I. D'Anessa, R. De Grandis, E. Varanda, V. M. Deflon, A. Desideri and A. A. Batista, *Metallomics*, 2016, **8**, 179; (*b*) R. S. Corrêa, M. M. da Silva, A. E. Graminha, C. S. Meira, J. A. F. dos Santos, D. R. M. Moreira, M. B. P. Soares, G. Von Poelhsitz, E. E. Castellano, C. Bloch Jr, M. R. Cominetti and A. A. Batista, *J. Inorg. Biochem.*, 2016, **156**, 153.
13 (*a*) M. I. F. Barbosa, R. S. Corrêa, K. M. de Oliveira, C. Rodrigues, J. Ellena, O. R. Nascimento, V. P. C. Rocha, F. R. Nonato, T. S. Macedo, J. M. Barbosa-Filho, M. B. P. Soares and A. A. Batista, *J. Inorg. Biochem.*, 2014, **136**, 33; (*b*) M. I. F. Barbosa, R. S. Correa, T. M. Bastos, L. V. Pozzi, D. R. M. Moreira, J. Ellena, A. C. Doriguetto, R. G. Silveira, C. R. Oliveira, A. E. Kuznetsov, V. S. Malta, M. B. P. Soares and A. A. Batista, *New J. Chem.*, 2017, **41**, 4468.
14 M. I. F. Barbosa, R. S. Corrêa, L. V. Pozzi, E. O. Lopes, F. R. Pavan, C. Q. F. Leite, J. Ellena, S. P. Machado, G. von Poelhsitz and A. A. Batista, *Polyhedron*, 2015, **85**, 376.
15 R. S. Correa, K. M. de Oliveira, F. G. Delolo, A. Alvarez, R. Mocelo, A. M. Plutin, M. R. Cominetti, E. E. Castellano and A. A. Batista, *J. Inorg. Biochem.*, 2015, **150**, 63.
16 M. V. N. Rodrigues, R. S. Correa, K. L. Vanzolini, D. S. Santos, A. A. Batista and Q. Cass, *RSC Adv.*, 2015, **5**, 37533.
17 A. A. Batista, M. O. Santiago, C. L. Donnici, I. S. Moreira, P. C. Healy, S. J. Berners-Price and S. L. Queiroz, *Polyhedron*, 2001, **20**, 2123.
18 S. Queiroz, A. Batista, G. Oliva, M. Gambardella, R. Santos, K. Macfarlane, S. Rettig and B. James, *Inorg. Chim. Acta*, 1998, **267**, 209.
19 COLLECT, Data Collection Software, Nonius, Delft, The Netherlands, 1998.
20 Z. Otwinowski and W. Minor, in *Methods in Enzymology: Macromolecular Crystallography*, ed. C. W. Carter Jr and R. M. Sweet, Academic Press, New York, 1997, part a, vol. 276, p. 307.
21 G. M. Sheldrick, *Acta Crystallogr., Sect. A: Found. Crystallogr.*, 2008, **64**, 112.
22 P. Coppens, L. Leiserowitz and D. Rabinovich, *Acta Crystallogr.*, 1965, **18**, 1035.
23 L. J. Farrugia, *J. Appl. Crystallogr.*, 2012, **45**, 849.
24 C. F. Macrae, I. J. Bruno, J. A. Chisholm, P. R. Edgington, P. Mccabe, E. Pidcock, L. R. Monge, R. Taylor, J. van de Streek and P. A. Wood, *J. Appl. Crystallogr.*, 2008, **41**, 466.
25 S. A. Ahmed, R. M. Gogal and J. E. Walsh, *J. Immunol. Methods*, 1994, **170**, 211.
26 W. J. Geary, *Coord. Chem. Rev.*, 1971, **7**, 81.
27 F. T. Martins, R. S. Correa, A. A. Batista and J. A. Ellena, *CrystEngComm*, 2014, **16**, 7013.
28 G. Portalone, L. Bencivenni, M. Colapietro, A. Pieretti and F. Ramondo, *Acta Chem. Scand.*, 1999, **53**, 57.
29 (*a*) K. Nakamoto, *Infrared and Raman Spectra of Inorganic and Coordination Compounds*, Wiley-Interscience, New York, 5th edn, 1997; (*b*) J. S. Singh, *J. Mol. Struct.*, 2008, **876**, 127.
30 R. R. Kumar, R. Ramesh and J. G. Małecki, *New J. Chem.*, 2017, **41**, 9130.
31 J. Irvoas, A. Noirot, N. Chouini-Lalanne, O. Reynes and V. Sartor, *New J. Chem.*, 2013, **37**, 2324.
32 J. K. Barton, K. E. Erkkila and D. T. Odom, *Chem. Rev.*, 1999, **99**, 2777.
33 F. Xue, C.-Z. Xie, Y.-W. Zhang, Z. Qiao, X. Qiao, J.-Y. Xu and S.-P. Yan, *J. Inorg. Biochem.*, 2012, **115**, 78.
34 P. D. Ross and S. Subramanian, *Biochemistry*, 1981, **20**, 3096.
35 V. R. Silva, R. S. Corrêa, L. S. Santos, M. B. P. Soares, A. A. Batista and D. P. Bezerra, *Sci. Rep.*, 2018, **8**(1), 288.

